Research Article | Vol. 29, No. 17 / 16 Aug 2021 / Optics Express 27768
Optics EXPRESS

Experimental comparison of DSB and CS-DSB mmW formats over a hybrid fiber and FSO fronthaul network for 5G

J. BOHATA,[1,*] D. N. NGUYEN,[1] J. SPÁČIL,[1] M. KOMANEC,[1] B. ORTEGA,[2] L. VALLEJO,[2] Z. GHASSEMLOOY,[3] AND S. ZVÁNOVEC[1]

[1]*Department of Electromagnetic Field, Czech Technical University in Prague, Technicka 2, Prague 6, 166 27, Czech Republic*
[2]*Polytechnic University of Valencia, Camí de Vera, 46022 Valencia, Spain*
[3]*Northumbria University, 2 Sandyford Rd, NE1 8QH, Newcastle upon Tyne, UK*
[*]*bohatja2@fel.cvut.cz*

Abstract: The telecommunication world is experiencing the 5th generation (5G) networks deployment including the use of millimeter wave (mmW) frequency bands to satisfy capacity demands. This leads to the extensive use of optical communications, especially the optical fiber connectivity at the last mile access and the edge networks. In this paper we outline fiber and free space optics (FSO) technologies for use as part of the 5G optical fronthaul network. We investigate two different mmW transmission schemes based on (*i*) the conventional analog radio over fiber transmission using one Mach-Zehnder modulator (MZM) with double sideband (DSB) optical modulation, and (*ii*) an optical-based frequency doubling with one MZM biased at the null point to introduce carrier suppression DSB (CS DSB) transmission and second MZM used for data modulation. Both systems are assessed in terms of the error vector magnitude, signal-to-noise ratio, dynamic range and phase noise. We consider a configuration for the fronthaul network in the frequency range 2 (FR2) at 27 and 39 GHz with the scale of bandwidth up to 400 MHz with M-quadrature amplitude modulation and quadrature phase shift keying. Results are also shown for FR1 at 3.5 GHz. Moreover, we investigate for the first time the 5G new radio signal transmission under strong turbulence conditions and show the turbulence-induced FSO link impairment. We finally demonstrate the CS DSB scheme performs well under chromatic dispersion-induced fading for the frequency up to 40 GHz and single mode fiber length of 30 km, whereas the DSB format seems more appropriate for an antenna seamless transmission.

1. Introduction

The 5th generation (5G) wireless networks [1], which have been deployed since 2019, are expected to account for approximately 10% of the global mobile devices (i.e., 1.4 billion out of the total of 13.1 billion according to the CISCO forecast [2]) and connections in 2023. The networks transmission capacity, and thus the requirement for new resources, need to satisfy the increasing end users' demand for access to information, more specifically for the video streaming via smart devices. High frequencies are well recognized worldwide as being the key component for the high-speed 5G services. The use of the unlicensed frequency bands above 6 GHz in 5G (and beyond) networks, which is labeled as frequency range 2 (FR2), is one complementary option to the licensed bands to offer ultrahigh speed mobile broadband communications. The most promising bands in FR2 are 27 and 39 GHz [3] providing sufficient bandwidth and covering a reasonably large service area, although the main limitation is due to big losses experienced by the high frequencies free space propagation.

#434334 https://doi.org/10.1364/OE.434334
Journal © 2021 Received 16 Jun 2021; revised 29 Jul 2021; accepted 29 Jul 2021; published 12 Aug 2021

Optics EXPRESS

The use of high frequency bands, i.e., millimeter wave (mmW), together with the need for massive data capacity places high demands on the adopted wireless technologies in terms of reliability, cost, efficiency (power and bandwidth), and robustness. The mmW technology is most widely needed in ultra-dense urban areas and hot-spot regions (e.g., football stadiums etc.) where the use of cloud radio access network (C-RAN) architecture has been considered as an interesting solution to save resources [4]. In C-RAN architectures, the baseband units (BBUs), hosted in the central office (CO), and the remote radio heads (RRHs) are physically decoupled. The RRH, which is kept at the base station (BS), and BBU, which is moved to the cloud infrastructure, are connected via an optical fronthaul network with increased demands on coverage, capacity and reduced latency and pressure on core network operations. This can be effectively implemented in 5G and beyond networks by a seamless convergence of the optical fiber and wireless technologies as reported in [5]. In [6], the analog radio over fiber (RoF) technology was introduced by moving all baseband processing, analog-to-digital conversion, up-conversion and electrical-to-optical conversion to the CO and keeping only the optical-to-electrical conversion, filtering, and amplification in the remote stations with reduced complexity [7]. An overview of RoF technologies adopted for wireless systems with an emphasis on the C-RAN architecture is given in [8].

To enhance the optical networks deployment and flexibility, particularly in urban areas, the free space optics (FSO) technology is considered as a potential solution [9]. The FSO offers optical fiber-based systems features including very large bandwidth at unlicensed frequency bands, immunity to electromagnetic interference, etc. However, in line with other wireless technologies, FSO links performance is affected by the channel conditions (i.e., fog, haze, and more importantly atmospheric turbulence (AT)) [10]. The latter is caused by the thermal distribution along the light signal propagation in the air that results in time variant beam refraction and beam width changes, thus leading to irradiance fluctuations known as scintillation [11].

1.1. Related works

In the literature, several radio over fiber (RoF), i.e. standard single mode optical fiber (SMF), radio over FSO (RoFSO) and a combination of both links for transmission of mmW signals using different modulation schemes such as double-sideband (DSB) and carrier-suppressed double sideband (CS DSB) have been reported. In [12], a 25 GHz 16-quadrature amplitude modulation (QAM) DSB signal based on either direct or external modulation was transmitted over 100 m SMF and 50 m long outdoor mmW links with the signal bandwidth limited to 20 MHz only. In [13], a CS DSB scheme for doubling the frequency to obtain the 40 GHz mmW signal with a 2 GHz bandwidth over a 20 km SMF was experimentally demonstrated. However, the 32-QAM signal was only evaluated at the intermediate frequency (IF) of 2 GHz, not at 40 GHz. In [14], a simple RoF link (20 km) with 3.5 Gbps on-off keying, which is not used in 5G networks, downstream link using the 72 GHz mmW based on all-optical CS DSB frequency eightfold technique and only a single external Mach-Zehnder modulator (MZM) was reported. A 60 GHz 4- and 16-QAM DSB signals with a bandwidth up to 400 MHz over a SMF were investigated in [15]; however fiber distance was limited to a 1 km of SMF, which is relatively short for optical fronthauling in 5G. In [16], the transmission of the 5G new radio (NR) standard signal of 26 GHz 16-QAM DSB with a bandwidth of 400 MHz over a 12.5 km of SMF, as well as 1 and 8 m long FSO and RF wireless channels, respectively was reported. However, the link performance was not investigated under the AT.

It is worth mentioning that in [17], we reported a detailed investigation of the AT distribution for the FSO path in a hybrid SMF and FSO channel using CS DSB-based frequency doubling technique at 40 GHz with a 2 GHz bandwidth and using 16-QAM. In [18] and [19], we also demonstrated the transmission of 25 GHz QPSK and 16/64-QAM signals using CS DSB-based frequency doubling technique over SMF, FSO and RF wireless links focusing on the impact

Optics EXPRESS

of AT on the FSO link. The signal performance was directly evaluated at 25 GHz; however, we only used a LTE signal with a 20 MHz bandwidth and thus the potential toward incoming telecommunication standards is limited.

1.2. Contributions

From the literature reviews, no works have been reported on the followings:

1. Transmission of the 5G NR signal at the mmW frequency bands of 27 and 39 GHz with a bandwidth up to of 400 MHz over the hybrid SMF, FSO and mmW wireless link and the system evaluation.
2. Experimental investigation and comparison of 39 GHz mmW DSB and CS DSB with QPSK and 64/256-QAM over the hybrid SMF and FSO channels with AT.
3. Characterization of the spurious-free dynamic range (SFDR) and the phase noise for both setups.

To the best of authors' knowledge, in this work for the first time we investigate the transmission of 5G NR signals at 39 GHz for DSB and CS DSB schemes over the combined analog RoF and RoFSO link. In addition, we experimentally demonstrate the implementation of 5G optical fronthaul with the hybrid SMF and FSO link at 3.5, 27, and 39 GHz bands. The paper is organized as follows. The experimental schemes are described in section 2, while results and discussion are provided in section 3. Finally, a summary of the main results of the paper is presented in section 4.

2. Experimental setup

As mentioned above, we have tested two setups for performance comparison of the mobile mmW fronthaul network as illustrated in Fig. 1(a). Both setups employ a continuous wave (CW) laser signal source (CoBrite DX4) with 16 dBm of output optical power. In Setup A, representing a classic analog MPL with DSB modulation and direct detection (DD), a 5G NR mmW signal at a particular carrier frequency is produced by a vector signal generator (R&S SMW200A) and applied to the MZM (Optilab IML-1550-50-PM), which is biased at its quadrature point. The output optical power of the MZM is 7 dBm. In Setup B, a radio signal at the half of the target carrier frequency, i.e., 12.5 GHz for 27 GHz and 18.5 GHz for 39 GHz transmission, produced by a signal generator (R&S SMF100A) is applied to MZM1 (Fujitsu FTM7938EZ/201), which is biased at its null point. The carrier-suppressed DSB (CS DSB) signal is led to low-speed MZM2 (Covega 10TM 081), which is biased at its linear point and modulated by the 2 GHz IF data signal from a vector signal generator (R&S SMW200A). The externally modulated optical signal with a power of -2 dBm is launched into the optical channel for transmission. In both Setups, the optical signal is directly detected at the optical receiver (Rx) (Optilab PD 40) and the resulting converted signal is captured by a signal analyzer (R&S FSW) for performance assessment. In the case of setup B, the beating of the optical sidebands at the optical Rx generates the signal at the double frequency of the original signal, i.e., 25 and 37 GHz with an additional IF of 2 GHz. Note that, due to the lower output optical power level in Setup B, an erbium doped fiber amplifier (EDFA) is required while in Setup A, the EDFA is only used when the FSO link is included. The optical channel used in Setups A & B consists of a fixed 10 km long SMF reel, providing a satisfactory range for connection between a CO and RRH, and a 4 m long FSO link as depicted in Fig. 1(b), to demonstrate a proof of concept. The latter offers a flexible solution to establish connectivity in high-density urban areas where burying fibers is costly and time consuming. The FSO link is composed of the Tx and the Rx with optical doublet collimators (Thorlabs F810APC-1550) for

Optics EXPRESS

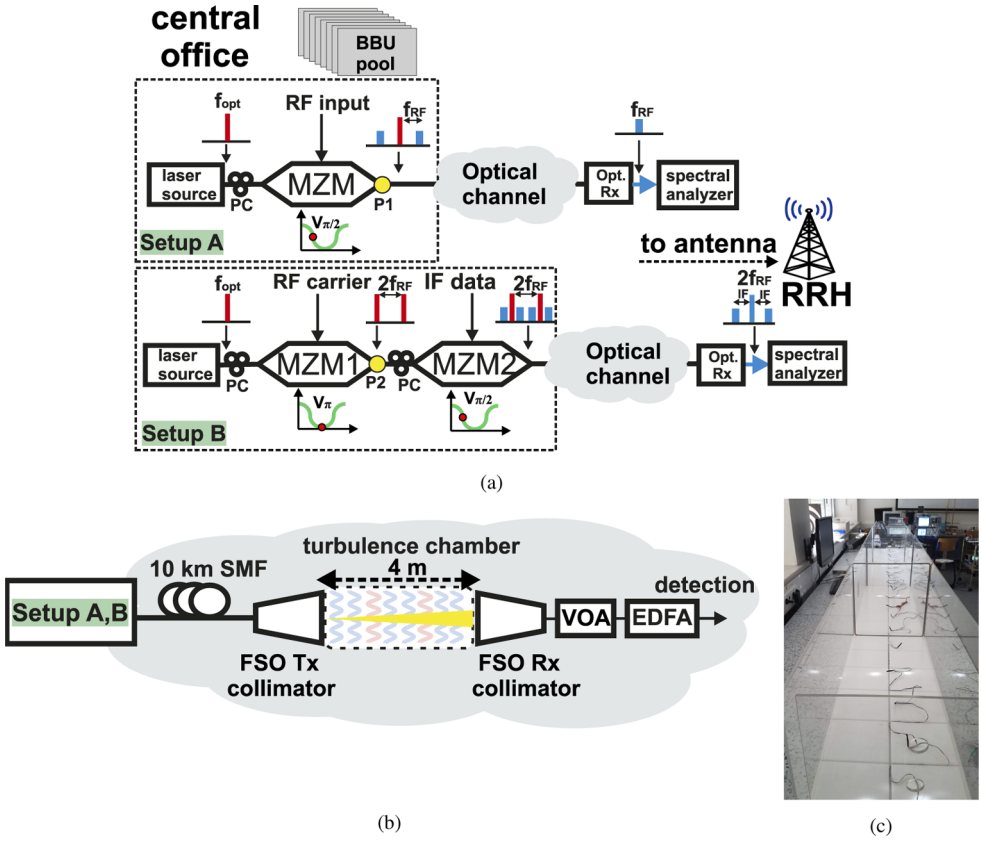

Fig. 1. (a) Setups A and B for an optical fronthaul network, (b) the full configuration of the optical channel, and (c) turbulent chamber.

launching and capturing the optical signal from and to the optical fiber, respectively. A laboratory AT chamber with controlled temperature distribution is employed for the FSO channel.

Table 1. System parameters

Parameter	Value
Laser wavelength	1550.6 nm
Laser output power	16 dBm
FSO length	4m
FSO loss	6 dB
FSO collimator aperture	2.4 cm
SMF length	10 km
SMF loss	2.5 dB
Opt. Rx responsivity	0.8 A/W
EDFA output power	3 dBm
EDFA noise figure	< 4 dB
PD bandwidth (-6dB)	> 40 GHz

Optics EXPRESS

Note that, in the FSO link the optical loss is 6 dB and a variable optical attenuator (VOA, Oz optics DA-100-SC-1300/1550-9/125-S-40) is used to control the input to the EDFA whose output power is set to 3 dBm. All the key parameters are summarized in Table 1.

3. Results and discussion

3.1. System characterization

The optical spectra with the RF carrier frequency of 27 GHz, measured in both Setups, are shown in Fig. 2. For Setup A, the spectrum captured in point P1 according to Fig. 1 evinces DSB optical modulation with sidebands located away from the optical carrier by the input RF, i.e., at 27 GHz, whereas Setup B shows the spectrum, obtained in point P2, of the suppressed carrier with two sidebands having the frequency difference between them equal to the double of the incoming electrical signal frequency to the modulator, which is 25 GHz in this case. Note that the original carrier frequency in Setup B is half, i.e., 12.5 GHz. Due to the absence of the optical carrier and beating of these sidebands at PD, a new RF carrier emerges in the frequency corresponding to the frequency difference between the sidebands, i.e., 25 GHz. Note, there is a second modulator MZM2 in Setup B, modulating data at the IF frequency of 2 GHz to the optical signal, so the total system output electrical carrier frequency is 27 GHz. Note that 2 GHz IF signal cannot be distinguished in optical spectral spectrum measured at the output of MZM2 even though we used high-quality spectral analyzer (Yokogawa AQ6370D), whose maximal resolution is 0.02 nm. Therefore, we have only shown the spectrum after MZM1 to demonstrate the transmission properties.

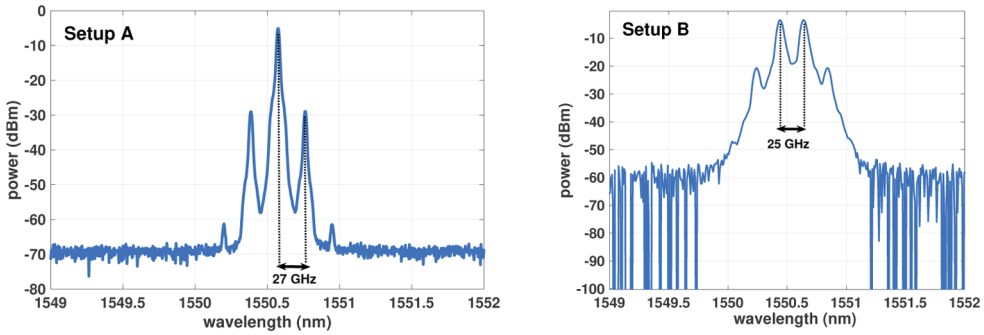

(a) (b)

Fig. 2. Optical spectra of the modulated optical signal for transmission at the frequency of 27 GHz for Setups: (a) A, and (b) B, which were obtained in points P1 and P2, respectively, according to Fig. 1(a).

Both setups have been characterized in terms of the spurious free dynamic range (SFDR) to demonstrate the impact of the third-order intermodulation distortion. For this purpose, we have used a two-tone test signal with 1 MHz spacing. It is worth to mention that, comparing to Setup A, the input power for the two-tone test in Setup B was applied to the the MZM2, i.e. low-frequency modulator, because the MZM2 is responsible for data modulation and thus most affects the overall performance. Measured results are depicted in Fig. 3. Note, in Setups A and B the noise floor levels are -158.0 and -156.5 dBm/Hz, respectively with the corresponding SFDR values of 88 and 89 dB $\times$ $Hz^{-2/3}$, respectively while there was employed EDFA in this test in Setup B. Based on the achieved results, both setups show very comparable dynamic range in terms of SFDR.

Optics EXPRESS

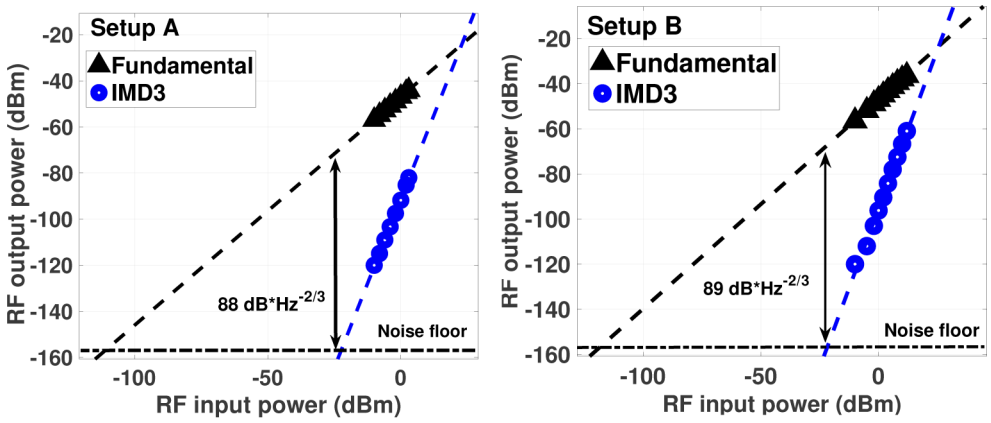

Fig. 3. Measured SFDR for Setups: (a) A, and (b) B.

For the overall system performance evaluation, 5G NR signals have been adopted according to the 3GPP 5G specifications in release 15, namely pre-defined test models TM1.1, TM3.1, and TM3.1a [20]. The test models use time division duplexing with a bandwidth range of 50 to 400 MHz, which is the maximum considered single bandwidth in 5G NR. These models are used, for example, for testing the output power dynamics or the quality of transmitted signal. Based on the 5G NR recommendations [21], we have selected frequency bands 3.5, 27, and 39 GHz for Setup A and 27 and 39 GHz for Setup B. Considering the fact that, the frequency multiplication technique (i.e., doubling) adopted in Setup B is preferably used only for higher frequency generation to relax the demands on the signal source, i.e., over 20 GHz, the frequency band 3.5 GHz has been tested only in the case of Setup A. Note that, the main focus is to characterize 27 GHz band, which is the closest band above FR1 for 5G, i.e., above 6 GHz [22]. The details of the adopted 5G NR signals are listed in Table 2. All used test models contain normal cyclic prefix with 14 OFDM symbols per slot.

Table 2. Used 5G NR signals – BW: bandwidth, ScS: subcarrier spacing, Thpt: throughput

Test model for 5G-NR	BW (MHz)	ScS (kHz)	CP (μ s)	Modul. Format	EVM limit (%)	Thpt (Mb/s)	Spectr. Eff. (b/s/Hz)
TM3.1	50	60	1.17	64QAM	9	178	3.56
TM3.1a	90	60	1.17	256QAM	4.5	444	4.93
TM3.1	100	60	1.17	64QAM	9	360	3.46
TM3.1	200	120	0.58	64QAM	9	692	3.46
TM3.1	400	120	0.58	64QAM	9	1386	3.47
TM3.1	400	120	0.58	QPSK	18.5	462	1.16

Note, (*i*) the highest throughput of 1.386 Gb/s is achieved at the bandwidth of 400 MHz and 64-QAM; and (*ii*) the best spectral efficiency of 4.93 b/Hz for a single channel without considering multiplexing techniques is at 90 MHz and 256-QAM, where the error vector magnitude (EVM) limit is the lowest i.e., 4.5 %.

3.2. *Chromatic dispersion-induced fading*

At first, we investigate the systems with only the SMF link (5 to 30 km) for (*i*) Setup A with no EDFA and an optical output power level of 7 dBm; and (ii) Setup B with EDFA, which is used to

Optics EXPRESS

compensate optical losses due to MZMs for the sake of comparison with Setup A. The EDFA output power is also 7 dBm and is placed behind the MZM2. Figure 4 depicts the EVM plots as a function of the SMF length for 400 MHz bandwidth quadrature phase shift keying (QPSK) and 200 and 400 MHz bandwidth 64-QAM signals for both setups at 27 GHz. The EVM limits of 9 and 18.5 % for QPSK and QAM, respectively, that are defined by 3GPP [20], are also shown in Fig. 4. For Setup A with optical DSB modulation format and with no filtering, we observe that the EVM limits are not met at fiber lengths of 5, 15 and 25 km, because of the chromatic dispersion, see marked measured points in Fig. 4.

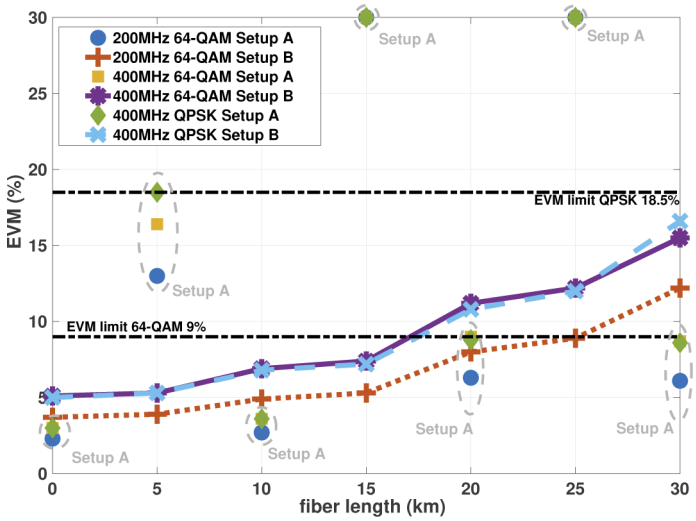

Fig. 4. The EVM versus SMF length for Setups A and B using QPSK and QAM with different bandwidth at 27 GHz.

The received optical power is the same for both Setups A and B. Considering an ideal intensity-modulated analog optical link, the RF signal transmission as a function of frequency will be constant. However, the transmission of the DSB signal evinces a substantial power drop in the RF spectrum due to the chromatic dispersion-induced fading. At the frequencies where RF response vanishes, intensity modulation of light is fully converted to the optical phase modulation, i.e., the optical intensity becomes constant, thus giving rise to no measurable RF response at the PD [6]. Setup B with the suppressed carrier displays maximal transmission link spans of (*i*) 17 and 25 km for 400 and 200 MHz 64-QAM, respectively for the EVM limits of 9%; and (*ii*) > 30 km for 400 MHz QPSK for the EVM limit of 18.5%.

The comparison of the RF frequency responses over a MPL with optical DSB and CS-DSB schemes, i.e. Setups A and B, respectively, for back to back (B2B) and different SMF lengths is shown in Fig. 5. For Setup B, the power transmission plots display a gradual decrease in the magnitude with the increasing SMF length, which follows the B2B plot, in contrast with Setup A, where a number of dips can be seen in the spectrum, which depends on the SMF lengths.

Considering the phase shift between both sidebands, the RF transmitted power corresponds to [23]:

$$P_{RF} \approx cos^2\left(\frac{\pi L D \lambda_0^2 f_{RF}^2}{c}\right) \tag{1}$$

where c is the light speed, L is the length of the fiber, D is the chromatic dispersion coefficient, λ_0 is the central optical wavelength and f_{RF} is the electrical frequency. Note, for the DSB schemes the chromatic dispersion induced power fading can be compensated, for example, by using a filter

Optics EXPRESS

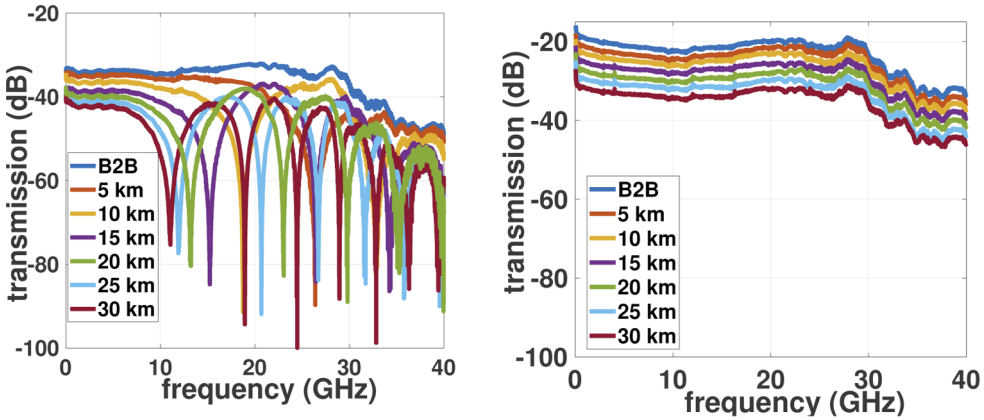

Fig. 5. The RF signal transmission response for different SMF lengths in: (a) Setup A, and (b) Setup B.

[24] to introduce optical single sideband transmission or by simultaneous intensity and phase modulation [25], but at the cost of increased complexity of the system.

3.3. *Full optical channel configuration with no AT*

Here, we consider both setups with a full configuration consisting of 10 km SMF and 4 m FSO link, as depicted in Fig. 1(b). Figure 6 shows the measured EVM values as a function of the data throughput at frequencies of 3.5, 27 and 39 GHz for Setup A and at 27 and 39 GHz for Setup B for QPSK and 64-QAM with the bandwidth range from 50 to 400 MHz. For Setup A, the EVM values are well below the limits for all cases at 3.5, 27 and 39 GHz, except for 400 MHz 64-QAM (highest data throughput of 1.4 Gb/s) at 39 GHz, which does not satisfy the 9 % threshold level. The same pattern is also observed in Setup B in Fig. 6(b), where all EVM values are below the limits except for 400 MHz 64-QAM at 39 GHz. It is worth to mention that for both 27 and 39 GHz tests, an optical Rx having lower frequency response at 39 GHz, compared to 27 GHz, was chosen.

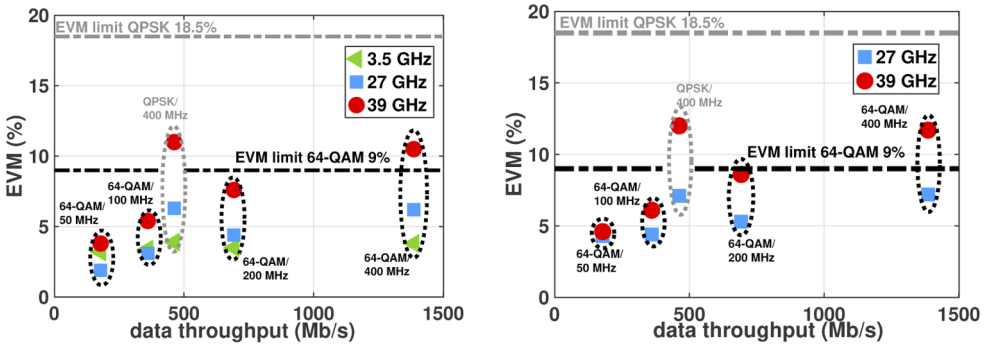

Fig. 6. Measured EVM after transmission over 10 km SMF and 4 m FSO optical channel for different signals and data throughput in: (a) Setup A, and (b) Setup B.

Presented results offer a better insight to the transmission capacity of fronthaul networks employing different MPL of SMF and FSO in comparison with digital fronthaul interface.

Optics EXPRESS

In another perspective, an appropriate modulation scheme and the signal bandwidth can be adopted to meet the data throughput requirement in 5G hybrid fronthaul links. Given that, 5G communication uses orthogonal frequency division multiplexing with the subcarrier spacing in the range of 15 to 120 kHz [26], the signal integrity in terms of the phase noise is critical. Characterizing and improving the phase noise performance of optically generated RF carrier signal is important for practical applications. Additive phase noise is the key parameter for accurately characterizing the phase noise due to the optical components [27,28]. Here, we show the phase noise performance for both microwave photonics setups, which are measured at the same frequencies and are illustrated in Table 3.

Table 3. Measured phase noise magnitudes for Setups A and B for the system with both SMF and FSO channels.

	Setup A			Setup B	
Frequency offset	@3.5 GHz (dBc/Hz)	@27 GHz (dBc/Hz)	@39 GHz (dBc/Hz)	@27 GHz (dBc/Hz)	@39 GHz (dBc/Hz)
1 kHz	-107	-108	-103	-99	-96
10 kHz	-102	-105	-109	-102	-100
100 kHz	-126	-118	-118	-110	-108
1 MHz	-136	-128	-127	-120	-121
10 MHz	-141	-132	-134	-132	-135

Note that, at the low frequency offset of 1 kHz Setup A offers improved phase noise by 7 to 10 dB compared with Setup B, whereas at the high frequency offset of 10 MHz, the phase noise levels are comparable in both cases. Figure 7 depicts the phase noise against the frequency offset for the optical channel composed of 10 km SMF and 4 m FSO at frequencies of 3.5, 27 and 39 GHz in Setup A and 27 and 39 GHz in Setup B, and also shows the results obtained for a B2B link for both setups. Note that, the performance varies with the carrier frequency significantly in Setup A, especially for the frequency offset < 1 MHz, while Setup B exhibits a minimal difference between 27 and 39 GHz over the given frequency offset and almost identical performance to that of B2B and the full channel compared with Setup A.

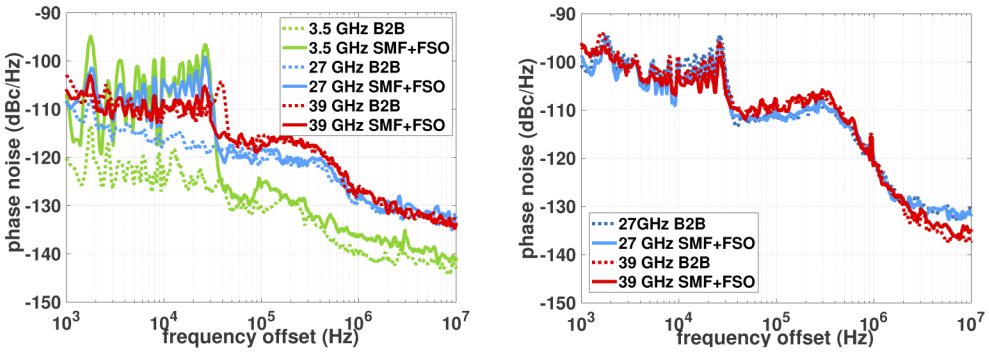

(a) (b)

Fig. 7. The phase noise performance for Setups: (a) A, and (b) B for 10 km SMF and 4 m FSO optical channel at different frequencies.

Next, we have investigated the EVM as a function of SNR for both setups at 27 GHz, as illustrated in Fig. 8. To measure the SNR, a combination of an electrical attenuator at the input stage and a signal analyzer at the Rx was adopted. Following the 5G NR standard, we evaluated 90 MHz bandwidth using 256-QAM, and 400 MHz bandwidth using QPSK and 64-QAM. As

Optics EXPRESS

expected, the EVM results for QPSK and 64-QAM show similar trends in both setups, since they have identical bandwidth of 400 MHz, however, each is subject to a different EVM limit. The highest required SNR is observed for 256-QAM. This is because the bandwidth is only 90 MHz comparing to 400 MHz for a fixed RF input power, i.e., 7 dBm, resulting in the highest power spectral density compared to the 400 MHz bandwidth. The 256-QAM transmission in Setup A offers improved performance in terms of the gain in the maximum SNR by 6 dB, and lower EVM by 2% compared with Setup B. In Setup A, the lowest EVM values of 1.3 and 2.1 % at the SNR of 35 dB are observed for 256-QAM/QPSK, and 64-QAM, respectively. In Setup B, the lowest EVM values are achieved at SNR of 28 and 35 dB for 64-QAM/QPSK, and 256-QAM, respectively. Thus in both setups, 256-QAM with 90 MHz bandwidth offers the best performance in terms of EVM, which is confirmed by the constellations shown for the selected SNR values.

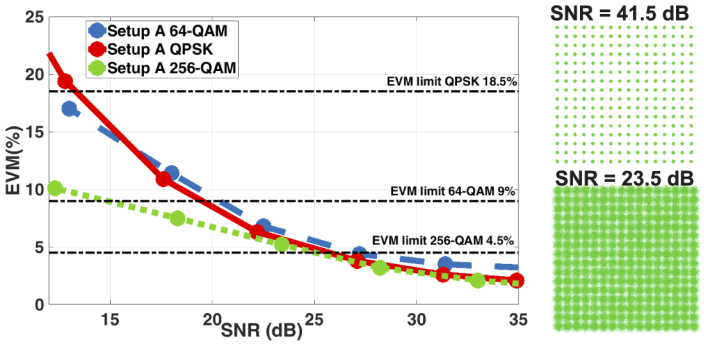

(a)

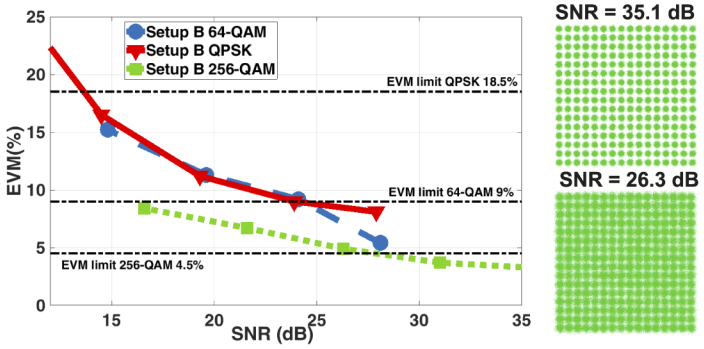

(b)

Fig. 8. EVM versus the SNR at 27 GHz for: (a) Setup A, and (b) Setup B. Inset are the constellations for 256-QAM at maximum SNR values and behind the edge of the EVM limit.

3.4. Full optical channel configuration with AT

As stated in the introduction, the FSO channel is affected by the atmospheric conditions including AT, which can lead to significant fluctuations of both amplitude and phase of the optical signal and thus leading to performance deterioration [29]. In this work, we have emulated a turbulent channel using an indoor atmospheric chamber. For this purpose, we have used (*i*) 20 temperature sensors, spaced 20 cm apart, which were placed within the chamber along the optical propagation path; (*ii*) two fan heaters blowing hot air perpendicular to the optical beam to generate a thermal gradient; and accordingly, the AT strength is calculated by using the equations given in [17]. To investigate the impact of different AT levels (i.e., scintillation index, which is proportional to

Optics EXPRESS

Rytov variance σ_R^2) on the hybrid link in a 5G fronthaul optical network, we have used weak (T0) and strong (T1) AT regimes defined by the refractive index structure parameter C_n^2 of 5.54×10^{-14} $m^{-2/3}$($\sigma_R^2 = 8.78\times10^{-6}$) and 1.15×10^{-11} $m^{-2/3}$ ($\sigma_R^2 = 1.83\times10^{-3}$), respectively. Note that, these values can be recalculated through σ_R^2 [10] for longer transmission spans maintaining the overall scintillation effect. For example, if we consider common FSO distances of 100 and 500 m in urban areas, then we have the turbulence levels of T0 with C_n^2 of 1.52×10^{-16} and 7.93×10^{-18} $m^{-2/3}$ and T1 with 3.14×10^{14} and 1.65×10^{-15} $m^{-2/3}$, respectively. The QPSK and 64-QAM signals with the 400 MHz bandwidth at 27 GHz were transmitted to compare the EVM performance under turbulence conditions as a function of SNR in both setups, see Fig. 9.

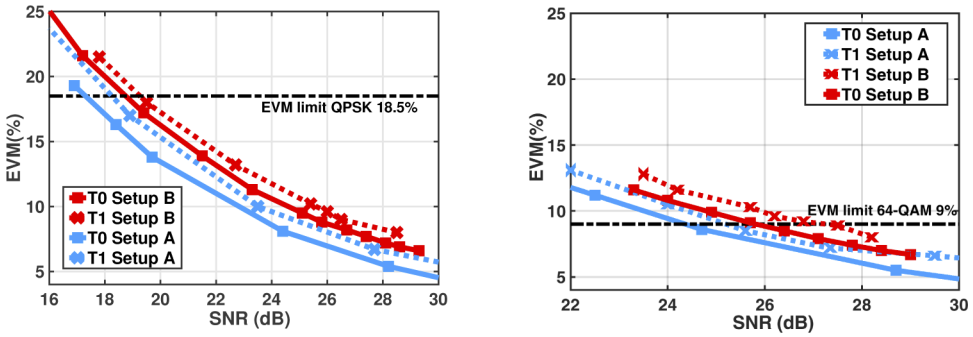

Fig. 9. EVM against SNR for Setups A (blue) and B (red) at 27 GHz with a 400 MHz of bandwidth for weak and strong AT regimes for: (a) QPSK, and (b) 64-QAM.

Note, the optical loss along the links was adjusted by using VOA. Once again, we observe that Setup A offered the highest SNR of 36 dB (not shown in Fig. 9 due to the limited x-axis scale) for both modulation schemes, and lower average EVM by 3 and 1% for QPSK and 64-QAM, respectively, compared with Setup B. Under AT and for a given SNR, the average EVM increased by 2 and 1% for QPSK and 64-QAM, respectively. In any case, we have shown that EVM values are below the EVM thresholds for both setups and modulation formats even under the strong AT regime. Figure 10 depicts the electrical power spectra for Setup A with 400 MHz 64-QAM for T0 and T1. Note, the in-band power variation of $\pm2-3$ dB around the average electrical received power value of -77 dBm for the case with T1 (orange curve) compared to T0 (grey curve), which is highly stable, i.e., flatter. The similar power variation in electrical spectrum under turbulence conditions in FSO channel has been observed e.g., in [17].

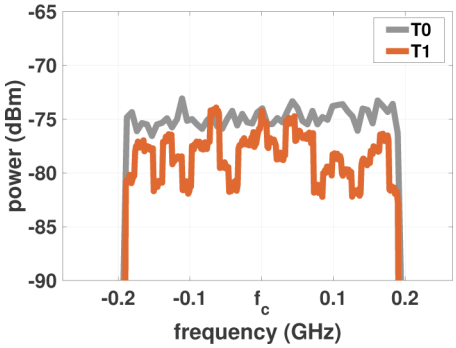

Fig. 10. Electrical spectra for Setup A with 400 MHz/64-QAM for T0 and T1.

Optics EXPRESS

Finally, we investigate the impact of AT on the EVM performance of both setups at 39 GHz for QPSK with the 400 MHz bandwidth. As depicted in Fig. 11, EVM shows a linear trend with reduced SNR for all cases and marginal difference between T0 and T1 compared with the case at 27 GHz. At the EVM limit of 18.5 %, the SNR penalties are within the range of 0.2-0.5 dB with the highest and lowest observed between T0 and T1 for Setups A and B, respectively. In particular, Setup B evinces very comparable EVM dependence on SNR for both low and strong turbulence regimes at 39 GHz. However, under strong turbulence conditions, there is about 1 dB lower maximal achieved SNR.

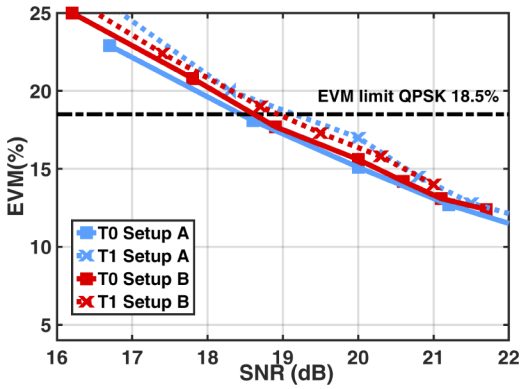

Fig. 11. EVM against SNR for Setups A (blue) and B (red) at 39 GHz with 400 MHz QPSK for T0 and T1 turbulence regimes.

3.5. Discussion and implementation

Two selected MPL systems' performances have been evaluated for the mobile fronthaul network application. In addition to the results shown along the paper, requirements and problems of RF antenna seamless transmission following optical-to-electrical conversion at the PD have to be taken into account for proper discussion.

The insignificant difference in the EVM performance between both setups under AT at 39 GHz highlights the advantage of Setup B with doubling of the original frequency (i.e., 18.5 GHz with 2 GHz of IF), and high frequency mmW signal transmission with the reduced phase noise. In other words, even though Setup B has some limitation, as discussed above, it shows a good performance for higher frequencies with the benefit of reduced requirements for RF equipment and less sensitivity to the chromatic dispersion-induced fading. The latter is crucial in systems with the DSB schemes at high frequencies employing long SMF, i.e., over 5 km, section. However, in Setup B using the carrier suppressed mode, there is a need for higher carrier suppression ratio (i.e., at least 20 dB) with sufficient optical and RF power levels to generate a strong electrical carrier at twice the original frequency. Moreover, the optical carrier is never completely suppressed. Also, the MZM2 is fed by the useful data signal with the IF offset, whose power is split (*i*) dominantly to DSB modulation at the new frequency; and (*ii*) then partially to DSB modulation at the residual original electrical frequency and a minimum to a frequency equal to the IF offset originated from the residual of the optical carrier. As a result, following optical transmission and the beating of the sidebands at the PD, a RF signal with a very strong carrier signal and two less powerful sidebands at the desired frequencies are generated. To transmit the signal via the free space path using the antenna relay, the signal needs to be amplified using at least a single RF amplifier on both the Tx and the Rx. However, by doing so the amplifier (or other active RF devices) may be overloaded by too strong carrier signal and the cost of lower power level for the data signal. Consequently, the data signal bandwidth, comparing to the RF

Optics EXPRESS

carrier, is not sufficiently amplified for antenna transmission and thus leading to lower SNR and worse EVM performance. This is more critical when large bandwidth signals are employed. Here, we bring part of our tests carried out along the experimental scenario, which have not been shown yet in the paper.

For example, in Setup B for the optical B2B configuration with an additional 3.5 m long RF link (antennas RFspin DRH40 with a gain of 15 dBi at 27 GHz) with two electrical amplifiers (Miteq AMF-4F-260400-40-10p), the measured received electrical power was about -33 dBm for 64-QAM with the 100 MHz bandwidth. The same amount of power was however assigned also for the 200 and 400 MHz bandwidth resulting in lower power spectral densities of 3 and 6 dB, respectively, which cannot be effectively compensated by amplification from the aforementioned reasons related with too strong RF carrier. More specifically, for the 400 MHz 64-QAM B2B link with no SMF and FSO links, the measured EVM following mentioned antenna transmission was 5.1%, which is below the EVM limit of 9%. However, increasing the optical path loss to 4 dB (e.g., corresponding to the loss of 20 km of SMF) by using the VOA, the received RF power is decreased by 8 dB with the EVM value of 10.6%, which is already above the EVM limit. This is adverse especially for higher bandwidth, i.e., $\geq$ 200 MHz, in contrast to much lower narrower bandwidth, i.e., 20 MHz, which can operate over relatively long free space path with much lower EVM as was demonstrated in [30]. This issue can, for example, be avoided using filtering to transform the spectrum to the electrical single side-band with the suppressed carrier signal. Note that, biasing MZM at its null transmission point results also in higher optical loss, which requires the use of EDFA in Setup B at the increased noise level and high costs. It has been verified that, the optimal optical power level at receiver for this configuration is at least 3 dBm to ensure the 64-QAM EVM limit with 400 MHz bandwidth. Note that, by including the mmW wireless link, the optical power requirement would be even higher. The optical channel (i.e., 4 m FSO and 10 km SMF) exhibits a loss of about 8.5 dB, and the two-MZM cascade introduces an additional loss of 18 dB. Therefore, without EDFA, the transmit power needs to get higher by at least 13.5 dB to main the link performance (i.e., the laser output power is 16 dBm). This can be achieved by using higher power lasers, but in risk of high power handling, or by adopting phase modulation (i.e., external modulation of the light signal) instead of intensity modulator to minimize the MZM loss. Nevertheless, Setup B (*i*) the CS-DSB scheme is immune to the chromatic dispersion-induced fading; (*ii*) offers improved stability under strong AT; (*iii*) maintains the same phase noise magnitudes across the frequency range; and (*iv*) significantly reduces requirements for the high frequency equipment, i.e., optical modulator and RF generators, thus reduces costs. Therefore, MZM at 18.5 GHz could be used instead of MZM at 39 GHz. Note, the same also applies to the both active and passive RF devices at the transmitter side.

On the other hand, Setup A, using a classic analog approach with a single MZM biased in the linear point with DD, represents a simple and universal solution for seamless RF signal transmission, i.e., 5G, over a fronthaul network even for high frequency mmW signals. Moreover, Setup A exhibits a 9 dB lower loss, comparing to Setup B, which implies the potential implementation of it without the need for EDFA under certain conditions. However, the drawbacks are the need to eliminate the chromatic-induced fading and the use of high frequency components. To conclude, both systems are applicable as an effective approach in 5G C-RAN each with its advantages and disadvantages as discussed above.

4. Conclusion

The experimental comparison of two MPL approaches for the 5G fronthaul network based on SMF and FSO links to transmit the 5G NR signal in different frequency bands was presented. We evaluated the performance of two setups using a conventional DSB analog MPL approach with an externally modulated laser and a CS DSB scheme to double the input carrier frequency, respectively, considering the data throughput, fiber chromatic dispersion, phase noise, SNR and

Optics EXPRESS

AT. We showed that, the CS DSB approach offered immunity to chromatic dispersion-induced fading for the frequency range up to 40 GHz and a SMF length of 30 km. We evinced no significant difference in the performance at 27 and 39 GHz thus making it as an attractive solution for higher frequency bands. Moreover, the CS-DSB scheme can be implemented with frequency n-multiplication to further relax the bandwidth requirements. Contrary, although the conventional DSB analog MPL approach is highly sensitive to dispersion-induced fading and requires higher bandwidth, it offers improved EVM performance since MZM is biased at the quadrature point instead of the null point as in CS DSB, higher SNR, lower phase noise, and reduced complexity. In addition, it was shown seamless deployment of antennas is another important issue, which needs to be considered especially in links with a large bandwidth ($\geq$ 200 MHz). To conclude, we showed that both approaches can operate at 27 and 39 GHz with the bandwidth up to 400 MHz even under the strong turbulence regime. Based on the measured results and validated by the analytical data, the EVM performance fulfilling the limit was achieved for the 500 m long outdoor FSO link under a moderate turbulence level (i.e., $C_n^2 = 1.65 \times 10^{-15}$ m$^{-2/3}$). The highest achieved data throughput was 1.4 Gb/s, which is sufficient for the chosen unlicensed single band. Finally, we proved that up to 256-QAM could be used in the proposed scheme with the hybrid SMF and FSO fronthaul network.

Funding. European Cooperation in Science and Technology (CA19111); Ministerstvo Průmyslu a Obchodu (FV40089); České Vysoké Učení Technické v Praze (SGS20/166/OHK3/3T/13).

Disclosures. The authors declare no conflicts of interest.

Data availability. Data underlying the results presented in this paper are not publicly available at this time but may be obtained from the authors upon reasonable request.

References

1. D. He, W. Wang, Y. Xu, X. Huang, H. Cheng, X. Duan, Y. Huang, H. Hong, Y. Zhang, and W. Zhang, "Overview of physical layer enhancement for 5G broadcast in release 16," IEEE Trans. Broadcast. **66**(2), 471–480 (2020).
2. CISCO, "Cisco Annual Internet Report (2018–2023) White paper," https://www.cisco.com/c/en/us/solutions/collateral/executive-perspectives/annual-internet-report/white-paper-c11-741490.html.
3. G. Gampala and C. J. Reddy, "Design of millimeter wave antenna arrays for 5G cellular applications using FEKO," in *2016 IEEE/ACES International Conference on Wireless Information Technology and Systems (ICWITS) and Applied Computational Electromagnetics (ACES)*, (2016), pp. 1–2.
4. T. R. Raddo, S. Rommel, B. Cimoli, and I. T. Monroy, "The optical fiber and mmwave wireless convergence for 5G fronthaul networks," in *2019 IEEE 2nd 5G World Forum (5GWF)*, (2019), pp. 607–612.
5. P. T. Dat, A. Kanno, N. Yamamoto, and T. Kawanishi, "Seamless convergence of fiber and wireless systems for 5G and beyond networks," J. Lightwave Technol. **37**(2), 592–605 (2019).
6. V. Urick, K. Williams, and J. McKinney, *Fundamentals of Microwave Photonics*, Wiley Series in Microwave and Optical Engineering (Wiley, 2015).
7. S. Rommel, D. Dodane, E. Grivas, B. Cimoli, J. Bourderionnet, G. Feugnet, A. Morales, E. Pikasis, C. Roeloffzen, P. van Dijk, M. Katsikis, K. Ntontin, D. Kritharidis, I. Spaleniak, P. Mitchell, M. Dubov, J. B. Carvalho, and I. Tafur Monroy, "Towards a scaleable 5G fronthaul: Analog radio-over-fiber and space division multiplexing," J. Lightwave Technol. **38**(19), 5412–5422 (2020).
8. D. Novak, R. B. Waterhouse, A. Nirmalathas, C. Lim, P. A. Gamage, T. R. Clark, M. L. Dennis, and J. A. Nanzer, "Radio-over-fiber technologies for emerging wireless systems," IEEE J. Quantum Electron. **52**(1), 1–11 (2016).
9. J. Bohata, M. Komanec, J. Spáčil, Z. Ghassemlooy, S. Zvánovec, and R. Slavík, "24-26 GHz radio-over-fiber and free-space optics for fifth-generation systems," Opt. Lett. **43**(5), 1035–1038 (2018).
10. L. Andrews and R. Phillips, *Laser Beam Propagation Through Random Media*, Online access with subscription: SPIE Digital Library (Society of Photo Optical, 2005).
11. N. A. M. Nor, Z. Ghassemlooy, J. Bohata, P. Saxena, M. Komanec, S. Zvanovec, M. R. Bhatnagar, and M.-A. Khalighi, "Experimental investigation of all-optical relay-assisted 10 Gb/s FSO link over the atmospheric turbulence channel," J. Lightwave Technol. **35**(1), 45–53 (2017).
12. J. Bohata, M. Komanec, J. Spacil, R. Slavik, and S. Zvanovec, "Transmitters for combined radio over a fiber and outdoor millimeter-wave system at 25 GHz," IEEE Photonics J. **12**(3), 1–14 (2020).
13. L. Vallejo, B. Ortega, J. Bohata, S. Zvanovec, and V. Almenar, "Photonic multiple millimeter wave signal generation and distribution over reconfigurable hybrid SSMF/FSO links," Opt. Fiber Technol. **54**, 102085 (2020).
14. H. Zhang, L. Cai, S. Xie, K. Zhang, X. Wu, and Z. Dong, "A novel radio-over-fiber system based on carrier suppressed frequency eightfold millimeter wave generation," IEEE Photonics J. **9**(5), 1–6 (2017).

Optics EXPRESS

15. K. Kanta, A. Pagano, E. Ruggeri, M. Agus, I. Stratakos, R. Mercinelli, C. Vagionas, P. Toumasis, G. Kalfas, G. Giannoulis, A. Miliou, G. Lentaris, D. Apostolopoulos, N. Pleros, D. Soudris, and H. Avramopoulos, "Analog fiber-wireless downlink transmission of IFoF/mmWave over in-field deployed legacy pon infrastructure for 5G fronthauling," J. Opt. Commun. Netw. **12**(10), D57–D65 (2020).
16. C. H. d. S. Lopes, E. S. Lima, L. A. M. Pereira, R. M. Borges, A. C. Ferreira, M. Abreu, W. D. Dias, D. H. Spadoti, L. L. Mendes, and A. C. S. Junior, "Non-standalone 5G NR fiber-wireless system using FSO and fiber-optics fronthauls," J. Lightwave Technol. **39**(2), 406–417 (2021).
17. L. Vallejo, M. Komanec, B. Ortega, J. Bohata, D.-N. Nguyen, S. Zvanovec, and V. Almenar, "Impact of thermal-induced turbulent distribution along FSO link on transmission of photonically generated mmw signals in the frequency range 26–40 GHz," IEEE Photonics J. **12**(1), 1–9 (2020).
18. D.-N. Nguyen, J. Bohata, J. Spacil, D. Dousek, M. Komanec, S. Zvanovec, Z. Ghassemlooy, and B. Ortega, "M-QAM transmission over hybrid microwave photonic links at the K-band," Opt. Express **27**(23), 33745–33756 (2019).
19. D.-N. Nguyen, J. Bohata, M. Komanec, S. Zvanovec, B. Ortega, and Z. Ghassemlooy, "Seamless 25 GHz transmission of LTE 4/16/64-QAM signals over hybrid SMF/FSO and wireless link," J. Lightwave Technol. **37**(24), 6040–6047 (2019).
20. ETSI, "5G release description, release 15," ETSI, TS 138 141-1 v15.0.0 (2019).
21. A. Tikhomirov, E. Omelyanchuk, and A. Semenova, "Recommended 5G frequency bands evaluation," in *2018 Systems of Signals Generating and Processing in the Field of on Board Communications*, (2018), pp. 1–5.
22. M. Sung, S.-H. Cho, J. Kim, J. K. Lee, J. H. Lee, and H. S. Chung, "Demonstration of IFoF-based mobile fronthaul in 5G prototype with 28-GHz millimeter wave," J. Lightwave Technol. **36**(2), 601–609 (2018).
23. M. Oishi, Y. Nishikawa, S. Akiba, J. Hirokawa, and M. Ando, "2-dimensional beam steering by 2 × 3 photonic antenna using millimeter-wave radio over fiber," in *2013 IEEE International Topical Meeting on Microwave Photonics (MWP)*, (2013), pp. 130–133.
24. T. Bakhvalova, M. Belkin, M. Kamalian-kopae, and S. Turitsyn, "Correcting the chromatic dispersion of a fronthaul fiber link in millimeter-wave radio -over-fiber networks," in *27th Telecommunications Forum, TELFOR 2019*, (IEEE, United States, 2020), pp. 1–4. 2019 27th Telecommunications Forum (TELFOR) ; Conference date: 26-11-2019 Through 27-11-2019.
25. Y. Cui, K. Xu, J. Dai, X. Sun, Y. Dai, Y. Ji, and J. Lin, "Overcoming chromatic-dispersion-induced power fading in ROF links employing parallel modulators," IEEE Photonics Technol. Lett. **24**(14), 1173–1175 (2012).
26. P. K. Yadav, V. K. Dwivedi, B. T. Maharaj, V. Karwal, and J. P. Gupta, "Performance enhancement of 5G OFDM systems using modified raised cosine power pulse," Wirel. Pers. Commun. **106**(4), 2375–2386 (2019).
27. W. Li and J. Yao, "Investigation of photonically assisted microwave frequency multiplication based on external modulation," IEEE Trans. Microwave Theory Tech. **58**(11), 3259–3268 (2010).
28. J. Yao, "Microwave photonics," J. Lightwave Technol. **27**(3), 314–335 (2009).
29. J. Libich and S. Zvanovec, "Influences of turbulences in near vicinity of buildings on free-space optical links," IET Microw. Antennas Propag. **5**(9), 1039–1044 (2011).
30. J. Bohata, J. Spacil, D.-N. Nguyen, S. Zvanovec, L. Vallejo, and B. Ortega, "Radio over 50 km fiber and joint 80 m FSO/wireless links using photonic frequency doubling for 5G," in *2019 IEEE Global Communications Conference (GLOBECOM)*, (2019), pp. 1–6.